

# Multi-User Pilot Pattern Optimization for Channel Extrapolation in 5G NR Systems

Yubo Wan, *Graduate Student Member, IEEE*, An Liu, *Senior Member, IEEE*, and Tony Q. S. Quek, *Fellow, IEEE*

**Abstract**—Pilot pattern optimization in orthogonal frequency division multiplexing (OFDM) systems has been widely investigated due to its positive impact on channel estimation. In this paper, we consider the problem of multi-user pilot pattern optimization for OFDM systems. In particular, the goal is to enhance channel extrapolation performance for 5G NR systems by optimizing multi-user pilot patterns in frequency-domain. We formulate a novel pilot pattern optimization problem with the objective of minimizing the maximum integrated side-lobe level (ISL) among all users, subject to a statistical resolution limit (SRL) constraint. Unlike existing literature that only utilizes ISL for controlling side-lobe levels of the ambiguity function, we also leverage ISL to mitigate multi-user interference in code-domain multiplexing. Additionally, the introduced SRL constraint ensures sufficient delay resolution of the system to resolve multipath, thereby improving channel extrapolation performance. Then, we employ the estimation of distribution algorithm (EDA) to solve the formulated problem in an offline manner. Finally, we extend the formulated multi-user pilot pattern optimization problem to a multiband scenario, in which multiband gains can be exploited to improve system delay resolution. Simulation results demonstrate that the optimized pilot pattern yields significant performance gains in channel extrapolation over the conventional pilot patterns.

**Index Terms**—Pilot pattern optimization, channel extrapolation, multi-user, 5G NR.

## I. INTRODUCTION

Orthogonal frequency division multiplexing (OFDM) has been widely recognized as an efficient modulation method in wireless communication systems due to its high data rate transmission and its robustness against frequency selectivity [1]. In time division duplex (TDD) OFDM systems, the base station (BS) conducts channel estimation based on the received uplink pilot symbols transmitted from the user. The quality of the estimation hinges significantly on the strategic placement of the pilots across subcarriers.

In fifth-generation (5G) new radio (NR) systems, each user typically allocates and transmits pilot symbols (also known as Sounding Reference Signals (SRSs) in 5G NR systems) within a designated bandwidth part (BWP) due to limitations in transmission power, occupying merely a fraction of the overall system bandwidth for a given SRS period [2]. Additionally, 5G NR systems adopt an orthogonal multi-user SRS transmission

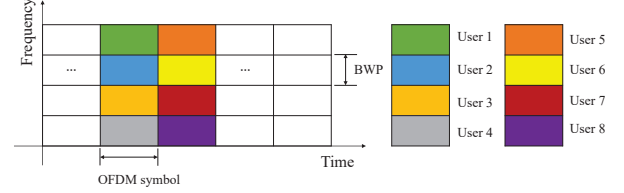


Fig. 1: An illustration of multi-user frequency-domain and time-domain multiplexing.

scheme employing three multiplexing methods: (1) **Code-Domain Multiplexing**. Users transmit SRSs on the same time-frequency resource using different Zadoff-Chu (ZC) pilot sequences [2]; (2) **Frequency-Domain Multiplexing**. Users transmit SRSs on distinct subcarriers within the same OFDM symbol; (3) **Time-Domain Multiplexing**. Users transmit SRSs on different OFDM symbols within the same BWP. These multiplexing methods are flexibly combined to increase the number of users supported by the system, as shown in Fig. 1.

Therefore, in 5G NR, the multi-user pilots transmission scheme merely estimates a subset of the uplink channels in frequency-domain for each user by utilizing received SRSs. This necessitates the application of extrapolation method to deduce the remaining channels. However, a new challenge arises: As compared to channel estimation, channel extrapolation relies more heavily on high-resolution channel parameter estimation to resolve the multipath components (MPCs) [3]. With the current pilot pattern adopted in 5G NR, the capability for channel extrapolation is constrained due to insufficient delay resolution resulting from the limited bandwidth of a BWP, which represents the bottleneck of current 5G NR systems. Numerous signal processing algorithms for channel extrapolation have been proposed [4]–[8], while research on pilot optimization to enhance channel extrapolation performance remains underexplored, particularly in multi-user scenarios.

A substantial amount of research has been dedicated to pilot pattern optimization in OFDM systems. The authors of [9] proposed a pattern design by maximizing the channel capacity, which took channel estimation errors into account. In [10], the pilot pattern is designed based on the minimization of the bit error ratio (BER). Moreover, a significant volume of research employed the mean squared error (MSE) of a channel estimator as a key metric for pilot pattern design, e.g., least squares (LS) estimator in [11], [12], least absolute shrinkage and selection operator (LASSO) estimator in [13], and linear minimum mean squared error (LMMSE) estimator in [14], [15]. Notably, reference [11] demonstrated that equi-powered and equi-spaced pilot-symbols lead to the lowest MSE of LS

This work was supported in part by National Key R&D Program of China (Grant No. 2021YFA1003304), in part by National Natural Science Foundation of China under Grant 62071416, and in part by Zhejiang Provincial Key Laboratory of Information Processing, Communication and Networking (IPCAN), Hangzhou 310027, China. (Corresponding author: An Liu.)

Yubo Wan, An Liu are with the College of Information Science and Electronic Engineering, Zhejiang University, Hangzhou 310027, China (email: wanyb@zju.edu.cn, anliu@zju.edu.cn).

T. Q. S. Quek is with the Singapore University of Technology and Design, Singapore 487372 (e-mail: tonyquek@sutd.edu.sg).

estimator. Furthermore, in scenarios where achieving an optimal pilot design is challenging due to time-varying channels, the authors in [12] proposed an adaptive pilot optimization scheme, yielding a suboptimal pilot arrangement.

Moreover, pilot optimization for sparse channel estimation has also been extensively investigated driven by the emergence of compressed sensing (CS) technology [16]–[19]. Minimizing mutual coherence of the measurement matrix has been widely employed for pilot optimization, e.g., [16], [17], [19], facilitating the exploitation of channel sparsity by CS-based algorithms. Besides, the authors in [18] adopted the MSE of channel estimation for sparse recovery algorithms as the optimization objective, which is averaged over all possible channel data available at the transmitter.

Nevertheless, several limitations are evident in the existing research:

- The majority of studies concentrate on single-user scenarios, where the designed pilot pattern may not be directly applicable to practical multi-user scenarios. Furthermore, in real communication systems such as 5G NR, code-domain multiplexing has to be considered for supporting more users. In multi-user scenarios, e.g., [20], however, the impact of pilot pattern on code-domain multiplexing of the systems has not been taken into account.
- Few studies explore pilot pattern optimization with the aim of enhancing multipath resolution capability of the systems for channel extrapolation. As explained before, channel extrapolation plays a crucial role in 5G NR systems and insufficient multipath resolution hinders channel extrapolation performance. However, most references pay attention to improve channel estimation accuracy through pilot optimization, but ignore the capability of the system to resolve MPCs. Particularly, the MSE of LS estimator and LMMSE estimator has been widely used for pilot pattern design, e.g., [11], [12], [14], [15]. Though LS and LMMSE estimators estimate the channel on the BWP that transmits SRS with high accuracy under the specially optimized pilot patterns, the extrapolation range of them is very limited [3].
- They mainly rely on the prior information of channel, e.g., realization of channel samples [13], [18], or precise channel statistical information [10], [14], [15]. However, acquiring such prior information is difficult in practical systems.
- Multiband technology has been widely employed in wireless systems, which combines multiple non-contiguous frequency bands to achieve high-resolution multipath delay estimation [21], [22]. Nonetheless, existing pilot pattern optimization in frequency-domain is typically based on a single contiguous frequency band, which cannot be applied to multiband scenarios.

Motivated by the limitations of existing pilot optimization methods and multi-user pilots transmission scheme employed in 5G NR, this paper proposes a novel scheme for the design of multi-user pilot pattern in uplink OFDM systems. We formulate a multi-user pilot pattern optimization problem and employ an evolutionary algorithm called estimation of distri-

bution algorithm (EDA) [16] to solve the formulated problem. This scheme addresses the issue of insufficient extrapolation capability in 5G NR systems and can be implemented in an offline manner. The optimized pilot pattern holds the potential to reduce multi-user interference caused by code-domain multiplexing and enhance the delay resolution of the system, thereby improving the overall channel extrapolation performance.

The main contributions of this paper are summarized as follows.

- 1) We formulate a novel pilot pattern optimization problem tailored for multi-user OFDM systems. The multi-user pilots are designed to minimize the worst integrated side-lobe level (ISL) [23] among users under the multi-user statistical resolution limit (SRL) constraint [24]. The performance metric, ISL, is derived from delay ambiguity function (AF) and can control the relative amount of energy in side-lobe portions with respect to the main-lobe portions of AF. As compared to existing methods that optimize the performance metrics such as MSE of channel estimation [13]–[15], minimizing ISL offers several advantages: (1) Enhanced delay estimation accuracy due to effective side-lobe suppression to mitigate the delay ambiguity [25]; (2) Improved multi-user interference cancellation capability in multi-user code-domain multiplexing, as explained in Subsection III-A1; (3) ISL optimization does not rely on any channel prior information. Then, the introduced SRL is a performance bound that provides a delay resolution limit for any practical method. The SRL constraint guarantees sufficient delay resolution of the optimized systems for channel extrapolation. The proposed optimization problem has the advantage of allowing offline optimization without prior information of the channel required.
- 2) The formulated multi-user pilot pattern optimization problem is extended to multiband scenarios, where the pilots are optimized across non-contiguous frequency bands/subcarriers. As compared to single-band scenarios, pilot optimization in multiband scenarios has the potential to enhance the delay resolution, aligning with our goal to improve channel extrapolation performance. Based on a formulated multiband signal model, we derive the corresponding ISL and SRL metrics in multiband multi-user scenarios and finally formulate the multiband multi-user pilot pattern optimization problem.
- 3) Extensive optimization results are presented in both single-band and multiband scenarios, considering the impact of multi-user interference on the system with both frequency-domain multiplexing and code-domain multiplexing. Particularly, the optimized pilot patterns have been presented, which can provide useful guidance for the pilot design in 5G NR systems. Superior channel extrapolation performance based on the optimized pilot pattern has been validated using realistic channels, i.e., the urban macro (UMa) scenario depicted in 3GPP R16 specifications [26].

The rest of this paper is organized as follows. In Section II,

we describe the system and signal model. In Section III, we firstly introduce the performance metrics ISL and SRL. Then, multi-user pilot pattern optimization problem is formulated and the adopted EDA algorithm to solve the formulated problem is introduced. In Section IV, the formulated problem is extended from single-band to multiband scenarios. Finally, simulation results and conclusions are given in Sections V and VI, respectively.

*Notations:* The notation  $\|\cdot\|_2$  denotes the  $\ell_2$ -norm,  $\text{diag}(\cdot)$  constructs a diagonal matrix from its vector argument, and  $*$  denotes the Hadamard product. The transpose, conjugate transpose, and inverse are denoted by  $(\cdot)^T$ ,  $(\cdot)^H$ ,  $(\cdot)^{-1}$  respectively. The notation  $\mathcal{N}(\mu, \Sigma)$  denotes a Gaussian normal distribution with mean  $\mu$  and variance  $\Sigma$ , and  $\mathbb{E}_{\mathbf{z}}[\cdot]$  denotes the expectation operator with respect to the random vector  $\mathbf{z}$ .

## II. SYSTEM AND SIGNAL MODEL

### A. System Model

Consider a multi-user OFDM system that adopts both code-domain multiplexing and frequency-domain multiplexing to support multi-user uplink transmission, as illustrated in Fig. II. In the considered system, each single antenna user transmits uplink SRSs to the BS. Note that the extension of our scenario to a user with multiple antennas is trivial, since the antennas in the same user are generally assigned with orthogonal SRSs. We employ the ZC sequences as the transmitted pilot symbols, which have been adopted in 5G NR and specified in 3GPP 5G NR Release 16 [2]. ZC sequences exhibit the useful property that cyclically shifted versions of themselves are orthogonal to one another. Specifically, the SRS sequence is generated by a cyclic shift of a base sequence, which is given by

$$r_u^\gamma(n) = e^{j\gamma n} \bar{r}_u(n), \quad (1)$$

where  $\bar{r}_u(n)$ ,  $n = 0, \dots, N - 1$ , is the base sequence,  $N$  denotes the number of subcarriers in full frequency band,  $u$  denotes the index number of the base sequence. The base sequence is cyclically shifted by the term  $e^{j\gamma n}$  to generate orthogonal sequences, which means that the inner product of  $r_u^\gamma(n)$  and  $\bar{r}_u(n)$  equals to zero. Generally, the pilot sequences are chosen from the orthogonality set  $\Gamma = \{\bar{r}_u(n), r_u^\gamma(n)\}$ ,  $\alpha \in \mathbb{Z}$ , to reduce the multi-user interference. However, the multi-user interference in code-domain multiplexing transmission not only relies on the orthogonality of the SRS sequences, but also relies on the multi-user pilot patterns in frequency-domain, which motivates the utilization of ISL to reduce multi-user interference in pilot pattern optimization, as detailed in Subsection III-A1.

### B. Pilot Signal Model

We consider  $G$  user groups with  $G$  pilot pattern vectors,  $\mathbf{w}_1, \dots, \mathbf{w}_G$ , and the users in the  $g$ -th group share the same pilot pattern vector  $\mathbf{w}_g$  but adopt different SRS sequences for supporting code-domain multiplexing. For the  $(g, z)$ -th user, i.e., the  $z$ -th user of the  $g$ -th user group, the channel frequency response (CFR) is given by

$$\mathbf{h}_{g,z} = \sum_{k=1}^{K_{g,z}} \alpha_{g,z,k} \mathbf{a}(\tau_{g,z,k}), \quad (2)$$

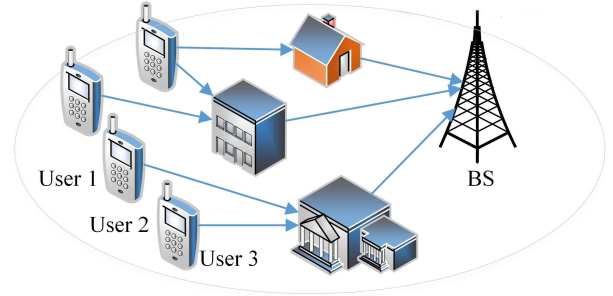


Fig. 2: Illustration of multi-user uplink system.

where

$$\mathbf{a}(\tau_{g,z,k}) = \left[ 1, e^{-j2\pi f_s \tau_{g,z,k}}, \dots, e^{-j2\pi(N-1)f_s \tau_{g,z,k}} \right]^T$$

denotes frequency-domain steering vector,  $\mathbf{h}_{g,z} \in \mathbb{C}^{N \times 1}$ ,  $K_{g,z}$  is the number of MPCs,  $f_s$  denotes the subcarrier spacing,  $\alpha_{g,z,k}$  and  $\tau_{g,z,k}$  denote the complex path gain and time delay of the  $k$ -th path, respectively. As our focus is on pilot pattern optimization in frequency-domain, which primarily impacts delay estimation performance, and considering that the different antennas of the BS receive equivalent training pilot sequences transmitted from the users, we consider CFR from a single antenna of the BS for simplicity.

In the pilot training phase, all users synchronously send their pilot signals to the BS. Then, the received signals in frequency-domain can be represented as

$$\mathbf{y} = \sum_{g=1}^G \sum_{z=1}^Z \text{diag}(\mathbf{w}_g * \mathbf{x}_z) \mathbf{h}_{g,z} + \mathbf{n}_{g,z}, \quad (3)$$

where  $\mathbf{y} \in \mathbb{C}^{N \times 1}$ ,  $\mathbf{x}_z \in \mathbb{C}^{N \times 1}$ ,  $z = 1, \dots, Z$ , denotes the  $z$ -th SRS sequence generated from (1), and  $\mathbf{n}_{g,z} \in \mathbb{C}^{N \times 1}$  denotes the additive white Gaussian noise (AWGN) with each element having zero mean and variance  $\sigma_{e,g,z}^2$ . We denote the number of non-zero elements of the pilot pattern vector  $\mathbf{w}_g \in \{0, 1\}^{N \times 1}$  as  $P_g$ . The non-zero elements in  $\mathbf{w}_g$  indicate the location of the transmitted SRS symbols of the  $g$ -th group in subcarriers and  $P_g$  represents the length of transmitted SRS sequence of the  $g$ -th group.

## III. MULTI-USER PILOT PATTERN OPTIMIZATION

In this section, we firstly elaborate the performance metrics ISL and SRL used in the multi-user pilot pattern optimization scheme. Then, we formulate the optimization problem and employ the EDA algorithm to solve this problem.

### A. Performance Metrics

1) *ISL:* The normalized ISL is defined as [23]

$$\text{ISL} \triangleq \frac{\int_{\mathcal{R}_s} |\chi(\Delta\tau)|^2 d\tau}{|\mathcal{R}_s| |\chi(0)|^2}, \quad (4)$$

where  $\chi(\Delta\tau)$  denotes the AF of the OFDM waveform at a given delay mismatch  $\Delta\tau \triangleq \tau_2 - \tau_1$ ,  $\mathcal{R}_s$  denotes the side-lobe region in the delay domain of the AF. Recalling the

observation model in (3), the AF of the  $(g, z)$ -th user can be derived as [23]

$$\begin{aligned}\chi_{g,z}(\Delta\tau) &= (\mathbf{w}_g * \mathbf{x}_z * \mathbf{a}(\tau_1))^H (\mathbf{w}_g * \mathbf{x}_z * \mathbf{a}(\tau_2)) \\ &= [(\mathbf{w}_g * \mathbf{w}_g) * (\mathbf{x}_z^* * \mathbf{x}_z)]^T [\mathbf{a}^*(\tau_1) * \mathbf{a}(\tau_2)] \\ &= \mathbf{w}_g^T \mathbf{a}(\Delta\tau).\end{aligned}\quad (5)$$

As can be seen, the AF is independent of the ZC sequences and thus we omit the subscript  $z$  as  $\chi_g(\Delta\tau)$  for the  $g$ -th group. From the definition of ISL, we can know that it characterizes the side-lobe levels of AF and does not rely on any prior information of the channel. This performance metric has been widely employed for waveform design in radar systems [23], [25], [27] to lower the side-lobe level. However, to the best of our knowledge, utilizing ISL to reduce multi-user interference in code-domain multiplexing for multi-user pilot transmission systems has not been studied yet.

Specifically, the multi-user system with code-domain multiplexing mitigates the multi-user interference by decoupling the received signal  $\mathbf{y}$  for each user in delay domain, which contains three steps:

(1) Multiply  $\mathbf{y}$  with the conjugation of the SRS sequence under the corresponding pilot pattern, e.g., for the  $(g, z)$ -th user,  $\tilde{\mathbf{y}}_{g,z} = \text{diag}(\mathbf{w}_g * \mathbf{x}_z^*) \mathbf{y}$ ;

(2) Transform  $\tilde{\mathbf{y}}_{g,z}$  into the delay domain by multiplying an inverse discrete Fourier transform (IDFT) matrix  $\mathbf{F}$ , i.e.,  $\tilde{\mathbf{y}}_{g,z}^D = \mathbf{F} \tilde{\mathbf{y}}_{g,z}$ ;

(3) Remove delays that are out of the delay spread region, i.e.,  $\hat{\mathbf{y}}_{g,z}^D = \mathcal{F} \{ \tilde{\mathbf{y}}_{g,z}^D \}$ .

A flow chart depicting the multi-user interference cancellation procedure is shown in Fig. 3. Note that though the original SRS sequences of two users may be orthogonal, the multi-user interference in code-domain multiplexing cannot be totally eliminated due to the impact of pilot patterns. Hence, after the above process of interference cancellation in delay domain, the multi-user interference is only partially eliminated, which motivates the utilization of ISL to design pilot pattern to further mitigate multi-user interference. The rationale behind the benefit of multi-user interference cancellation for code-domain multiplexing from the optimization of ISL is reasonable, since the cancellation of multi-user interference exactly occurs in delay domain, which aligns with the domain where ISL is defined.

To demonstrate the indication of ISL on interference cancellation, we present the magnitude curves of  $\tilde{\mathbf{y}}_{g,z}^D$  in Fig. 4 under two conventional pilot patterns, i.e., uniform pattern and random pattern, as illustrated in Fig. 5, where we set 4 users being divided into  $G = 2$  user groups and different user groups occupy different subcarriers. The interference between the two users in the same group is handled by code-domain multiplexing. We set  $P_g = 128, \forall g, N = 256, f_s = 120$  KHz. The channel has 2 paths with delays uniformly generated from  $[0, 400]$  ns for all users. The signal-to-noise ratios (SNR) is set as 15 dB. The averaged ISL value among users based on the uniform pattern and random pattern is  $-23$  dB and  $-21$  dB, respectively. As can be seen, the pattern scheme with lower ISL has less energy leakage from the main-lobe and thus has lower side-lobe level. Moreover, there is larger

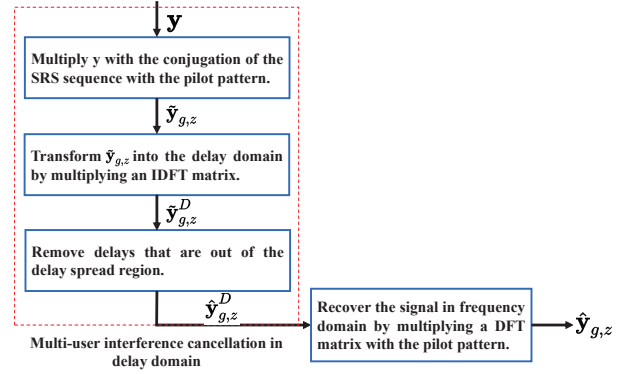


Fig. 3: The flow chart of the multi-user interference cancellation procedure.

multi-user interference for code-domain multiplexing due to energy leakage from user B to the delay spread region of user A for the random pilot pattern scheme due to the higher ISL.

Finally, we can recover the signal for each user in frequency-domain by multiplying a discrete Fourier transform (DFT) matrix with the corresponding pilot pattern as  $\hat{\mathbf{y}}_{g,z} = \mathbf{w}_g * (\mathbf{F}^H \hat{\mathbf{y}}_{g,z}^D)$ . The normalized mean square error (NMSE) (as defined in (21)) of the recovered channel in frequency domain for uniform pattern and random pattern scheme is 0.0085 and 0.3361, respectively. As indicated by the ISL, the uniform pattern scheme is less affected by the multi-user interference than the random pattern scheme, and thus leads to a better channel estimation performance.

Then, since ISL is also independent of the SRS sequence  $\mathbf{x}_z$  as the AF, we derive the closed-form expression of the ISL of the  $g$ -th group. Substituting (5) into (4), the ISL of the  $g$ -th group can be written as

$$\text{ISL}_g = \frac{\mathbf{w}_g^T \mathbf{G} \mathbf{w}_g}{|\mathcal{R}_s| (\mathbf{w}_g^T \mathbf{1})^2}, \quad (6)$$

where

$$\mathbf{G} = \int_{\mathcal{R}_s} \mathbf{a}(\Delta\tau) \mathbf{a}^H(\Delta\tau) d\tau. \quad (7)$$

For a symmetric interval  $\mathcal{R}_s \triangleq [-b, -a] \cup [a, b]$ ,  $a, b \in \mathbb{R}^+$ ,  $\mathbf{G}$  is a symmetric Toeplitz matrix and hence can be described by its first column  $\mathbf{f}(n)$ ,  $n = 0, \dots, N-1$ , where

$$\mathbf{f}(n) = \begin{cases} \frac{\sin(2\pi n f_s b) - \sin(2\pi n f_s a)}{\pi n f_s} & n = 1, \dots, N-1, \\ 2b - 2a & n = 0. \end{cases}$$

2) *Delay SRL*: The performance metric delay SRL is defined as [24]

$$\begin{aligned} \text{SRL} &\triangleq \Delta\tau \\ \text{s.t. } \Delta\tau &= \sqrt{\text{CRB}_{\Delta\tau}}, \end{aligned} \quad (8)$$

where  $\text{CRB}_{\Delta\tau}$  denotes the Cram er-Rao bound (CRB) for  $\Delta\tau$ . CRB serves as a MSE lower bound for the unbiased estimator [28]. The delay SRL is defined using the CRB of signal parameters for the cases where two path delays are closely located. According to the definition in (8), the delay SRL is the delay separation that is equal to its own

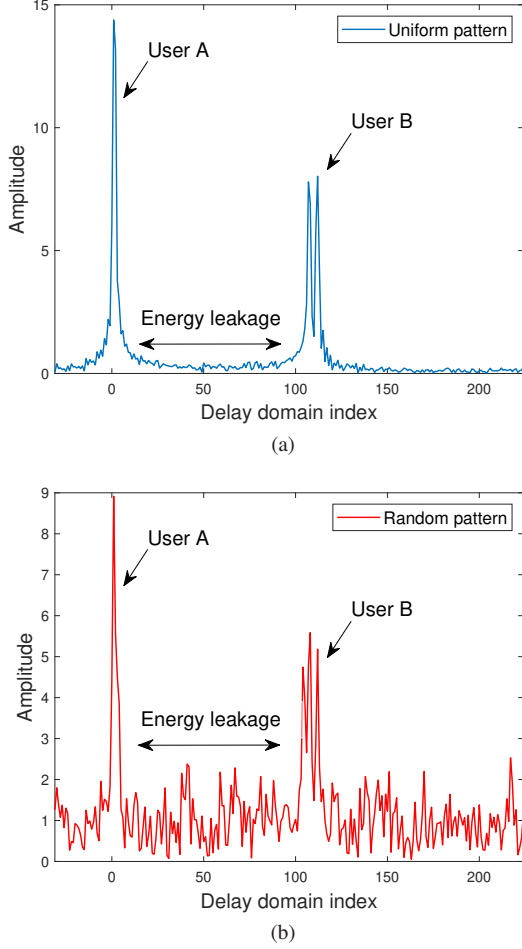


Fig. 4: An illustration of magnitude curves of a user group in delay domain.

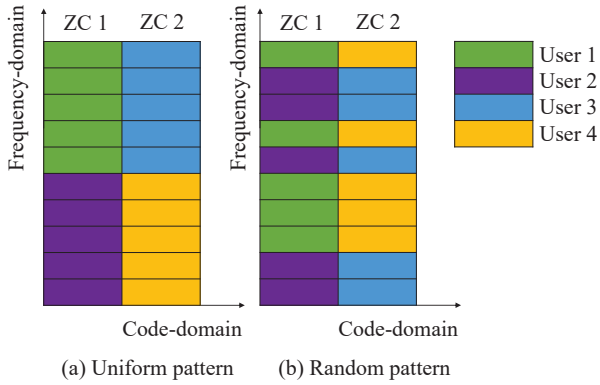


Fig. 5: An illustration of uniform pilot pattern and random pilot pattern.

root squared CRB. If there are multiple solutions in (8), the SRL can be defined as the smallest delay separation among all the solutions. In this definition, the delays can be exactly “resolved” when the standard deviation of the delay separation estimation is equal to the true separation. Delay SRL provides the highest delay resolution achievable by any

unbiased estimator.

Then, the CRB for the delay separation of the  $(g, z)$ -th user,  $\text{CRB}_{\Delta\tau_{g,z}}$ , is derived as

$$\begin{aligned} \text{CRB}_{\Delta\tau_{g,z}} &= \frac{\partial\Delta\tau_{g,z}}{\partial\boldsymbol{\theta}_{g,z}} \mathbf{J}_{\boldsymbol{\theta}_{g,z}}^{-1} \frac{\partial\Delta\tau_{g,z}}{\partial\boldsymbol{\theta}_{g,z}}, \\ &= \mathbf{J}_{\boldsymbol{\theta}_{g,z}}^{-1}(1,1) + \mathbf{J}_{\boldsymbol{\theta}_{g,z}}^{-1}(2,2) - \mathbf{J}_{\boldsymbol{\theta}_{g,z}}^{-1}(1,2) \\ &\quad - \mathbf{J}_{\boldsymbol{\theta}_{g,z}}^{-1}(2,1), \end{aligned} \quad (9)$$

where  $\mathbf{J}_{\boldsymbol{\theta}_{g,z}} \triangleq \mathbb{E}_{\mathbf{y}} \left[ -\frac{\partial^2 \ln f(\mathbf{y}|\boldsymbol{\theta}_{g,z})}{\partial\boldsymbol{\theta}_{g,z} \partial\boldsymbol{\theta}_{g,z}^T} \right]$  is the Fisher information matrix (FIM) associated with the vector  $\boldsymbol{\theta}_{g,z}$ ,  $f(\mathbf{y}|\boldsymbol{\theta}_{g,z})$  is the likelihood function of the random vector  $\mathbf{y}$  conditioned on  $\boldsymbol{\theta}_{g,z}$ , and  $\boldsymbol{\theta}_{g,z} \triangleq [\boldsymbol{\tau}_{g,z}^T, \boldsymbol{\alpha}_{g,z}^T]^T$  consisting of the unknown parameters:

$$\begin{aligned} \boldsymbol{\tau}_{g,z} &= [\tau_{g,z,1}, \tau_{g,z,2}]^T, \\ \boldsymbol{\alpha}_{g,z} &= [(\boldsymbol{\alpha}_{g,z}^R)^T, (\boldsymbol{\alpha}_{g,z}^I)^T]^T, \\ \boldsymbol{\alpha}_{g,z}^R &= [\alpha_{g,z,1}^R, \alpha_{g,z,2}^R]^T, \\ \boldsymbol{\alpha}_{g,z}^I &= [\alpha_{g,z,1}^I, \alpha_{g,z,2}^I]^T, \end{aligned} \quad (10)$$

in which  $\boldsymbol{\alpha}_{g,z}^R$  and  $\boldsymbol{\alpha}_{g,z}^I$  denote the real and imaginary parts of  $\boldsymbol{\alpha}_{g,z}$ , respectively. We set  $K_{g,z} = 2$  since delay SRL is exactly defined based on two close delays. Note that in practical scenarios with the number of multipath  $K_{g,z} > 2$ , the pilot pattern results of the adopted offline optimization can still be effective to improve the channel extrapolation performance, as verified by the numerical simulations in Section V. The reader is referred to Appendix A for detailed derivations of  $\mathbf{J}_{\boldsymbol{\theta}_{g,z}}$ .

### B. Problem Formulation

Generally, the uniform pilot pattern leads to a small ISL value, while the random pilot pattern leads to a small SRL value. However, channel extrapolation for multi-user requires the ISL to be as small as possible and the SRL cannot be too large. Therefore, we aim to minimize the maximum ISL among all users by pilot pattern optimization to improve the overall multi-user system performance. At the same time, a relatively small SRL should be guaranteed. Consequently, the problem can be formulated as

$$\begin{aligned} \mathcal{P}: \quad & \min_{\mathcal{X}} \max_g \{ \text{ISL}_g \} \\ & \text{s.t.} \quad \text{SRL}_{g,z} \leq \beta_{g,z}, \forall g, z, \\ & \sum_{g=1}^G \mathbf{w}_g \leq \mathbf{1}, \end{aligned} \quad (11)$$

where  $\mathcal{X} \triangleq \{\mathbf{w}_1, \dots, \mathbf{w}_G\}$  denotes the optimization variables set,  $\text{SRL}_{g,z}$  denotes the SRL of the  $(g, z)$ -th user, and  $\beta_{g,z}$  denotes the upper limit on the SRL of the  $(g, z)$ -th user. Minimizing ISL leads to less multi-user interference in code-domain and less delay ambiguity for delay estimation since the side-lobe of the AF is suppressed. Constraint (11) guarantees sufficient delay resolution of the multi-user system for channel extrapolation. Consequently, the multi-user system is expected to reach an enhanced channel extrapolation performance under the optimized multi-user pilot pattern of problem  $\mathcal{P}$ . Constraint

(12) ensures that the pilot symbols allocated to different users are not overlapped in subcarriers.

Note that the problem  $\mathcal{P}$  is optimized in an offline manner, which does not require any instantaneous realization of channel samples or prior information of channel statistical characteristics as other pilot pattern optimization schemes, e.g., [10], [13]–[15], [18]. Specifically, since the calculation of delay SRL requires true value of the noise variance and the path gains, we set the noise variance and the path gains of the users in the same group to be the same as a fixed value, i.e.,  $\sigma_{e,g,1} = \sigma_{e,g,2} = \dots = \sigma_{e,g,Z} = \sigma_g, \forall g$ ,  $\alpha_{g,1,k} = \alpha_{g,2,k} = \dots = \alpha_{g,Z,k} = \rho_{g,k}, \forall g, k$ , so that the users in the same group have the same SRL and the SRL can be readily calculated in an offline manner. Note that the setting value of  $\sigma_g$  and  $\rho_{g,k}$  have relatively little effect on the final channel extrapolation performance since we can adjust the corresponding  $\beta_{g,z}$  to ensure that the delay SRL constraint (11) is always effective to shape the pilot pattern. In other words, the optimal solution for  $\mathcal{P}$  under a typical value of  $\sigma_g, \rho_{g,k}, \beta_{g,z}$  can also achieve a pretty good channel extrapolation performance under a wide range of  $\sigma_g, \rho_{g,k}, \beta_{g,z}$ . In practice, we set  $\sigma_g, \rho_{g,k}$  to a typical SNR of 15 dB (In the simulations, we have set  $\rho_{g,1} = \rho_{g,2} = 1$ ,  $\sigma_g = 0.1778, \forall g$ ). For given  $\sigma_g$  and  $\rho_{g,k}$ , we calculate the SRL value under a random pilot pattern as a reference for setting  $\beta_{g,z}$ . It is because random pilot pattern generally leads to a much better SRL than other pilot pattern schemes. In Section V, the effectiveness of our proposed offline pilot pattern optimization scheme has been verified in a practical multipath channel model, which outperforms the benchmark schemes with significant performance gains.

Finally, substituting (6) and (8) into  $\mathcal{P}$ , the problem can be equivalently formulated as

$$\begin{aligned} \mathcal{P}: \quad & \min_{\mathcal{X}} \max_g \left\{ \frac{\mathbf{w}_g^T \mathbf{G} \mathbf{w}_g}{|\mathcal{R}_s| (\mathbf{w}_g^T \mathbf{1})^2} \right\} \\ & \text{s.t.} \quad \Delta\tau_g \leq \beta_g, \forall g, \\ & \quad \sqrt{\text{CRB}_{\Delta\tau_g}} = \Delta\tau_g, \forall g, \\ & \quad \sum_{g=1}^G \mathbf{w}_g \leq \mathbf{1}. \end{aligned}$$

Note that we omit the subscript  $z$  in the delay SRL constraint since the problem  $\mathcal{P}$  is independent of the subscript  $z$  in offline optimization. Pilot pattern optimization of  $\mathcal{P}$  is an integer nonlinear programming (INLP) problem. Finding the optimal solution of an INLP problem is intractable because it is generally non-deterministic polynomial-time hard (NP-hard). In next subsection, we will employ the EDA method to solve this problem.

### C. EDA for Solving $\mathcal{P}$

EDA is an evolutionary algorithm that operates by learning and sampling the probability distribution of the best individuals within a population at each generation. Unlike producing a specific individual, EDA introduces population diversity by sampling individuals from the probability distribution. This

characteristic endows EDA with a stronger global search ability and robustness compared to other evolutionary algorithms when solving INLP problems [16].

Generally, EDA starts with a random initialization of a population  $\mathcal{W}^{(0)}$  composed of  $Q$  individuals, i.e.,  $\mathcal{W}^{(0)} = \{\mathbf{W}_1^{(0)}, \dots, \mathbf{W}_Q^{(0)}\}$ , where  $\mathbf{W}_q^{(0)} \in \{0, 1\}^{N \times G}$  is a binary matrix representing a candidate of the multi-user pilot pattern matrix,  $\mathbf{W} \triangleq [\mathbf{w}_1, \dots, \mathbf{w}_G] \in \{0, 1\}^{N \times G}$ . Each row of  $\mathbf{W}_q^{(0)}$  has at most one non-zero element in order to satisfy constraint (12). In addition, only the samples satisfying constraint (11) are selected as the candidate individuals. The SRL is calculated by one-dimensional search of  $\Delta\tau$  in (8) with acceptable computational complexity.

Then, for the  $i$ -th iteration, we select the best  $T$  ( $T < Q$ ) individuals from  $\mathcal{W}^{(i-1)}$  denoted as  $\widetilde{\mathcal{W}}^{(i)} = \{\widetilde{\mathbf{W}}_1^{(i)}, \dots, \widetilde{\mathbf{W}}_T^{(i)}\}$ . The goodness of the individuals is measured by the objective function value in  $\mathcal{P}$  (also called fitness in EDA algorithms). In our problem, a smaller fitness (ISL value) indicates a better individual.

Next, we calculate the probability of a pilot symbol occurring on the  $n$ -th subcarrier of the  $g$ -th group by averaging among the individuals in  $\widetilde{\mathcal{W}}^{(i)}$ , i.e.,

$$p^{(i)}(n, g) = \frac{1}{T} \sum_{t=1}^T \widetilde{\mathbf{W}}_t^{(i)}(n, g). \quad (13)$$

Then, we generate a new population  $\mathcal{W}^{(i)}$  with individuals  $\mathbf{W}_q^{(i)}(n, g) \sim \text{Bern}(p^{(i)}(n, g))$ , where  $\text{Bern}(p^{(i)}(n, g))$  represents a Bernoulli distribution with probability  $P(\mathbf{W}_q^{(i)}(n, g) = 1) = p^{(i)}(n, g)$ , under the condition of satisfying constraints (11)–(12). Besides, we preserve the best individual from  $\mathcal{W}^{(i-1)}$  to  $\mathcal{W}^{(i)}$ . As the algorithm iterates,  $p^{(i)}(n, g)$  would converge to a stable distribution satisfying  $p^{(i)}(n, g) = 0$  or 1.

The EDA algorithm not only preserves the current best individual, but also introduces diversity by sampling the probability distribution to generate new individuals, and hence is able to escape from local optimums with high probability. The EDA algorithm for multi-user pilot pattern optimization is summarized in Algorithm 1.

## IV. EXTENSION TO MULTIBAND SCENARIOS

Multiband technology is proposed to achieve high-resolution delay estimation by jointly utilizing measurements from received OFDM signals across various non-contiguous frequency bands [21]. This technology aligns with our goal to enhance channel extrapolation performance and thus motivates the pilot pattern design in multiband scenarios to further improve delay resolution of the system.

As shown in Fig. 6, the spectrum resource used for pilot transmission consists of a number of non-contiguous frequency subbands in the presence of frequency band apertures, e.g.,  $f_{c,2} - f_{c,1}$ , with central frequencies  $f_{c,m}$  and subcarrier spacing  $f_{s,m}$  of the  $m$ -th subband. The frequency subbands allocated to other systems or applications are illustrated by the green color and cannot be utilized for pilot transmission. As discussed in [21], [22], the multiband gains originated from

**Algorithm 1** The EDA algorithm for multi-user pilot pattern optimization

**Input:**  $Q, T, \mathcal{R}_s, \beta_g, \sigma_g, \rho_{g,1}, \rho_{g,2}, \forall g$ , maximum iteration number  $I$ .

**Output:** The optimal pilot pattern matrix  $\mathbf{W}_{\text{best}}^{(I)}$ .

- 1: Randomly generate  $Q$  individuals of the pilot pattern matrix  $\mathbf{W}_q^{(0)}$  to initialize the population  $\mathcal{W}^{(0)}$ .
- 2: **for**  $i = 1, \dots, I$  **do**
- 3: Evaluate the fitness of individuals  $\mathbf{W}_q^{(i-1)}$  in  $\mathcal{W}^{(i-1)}$  by calculating the objective function of  $\mathcal{P}$ .
- 4: Select the best  $T$  individuals from  $\mathcal{W}^{(i-1)}$  to construct a new population  $\widetilde{\mathcal{W}}^{(i)}$ .
- 5: Calculate pilot occurrence probability matrix  $\mathbf{P}^{(i)} \in \mathbb{R}^{N \times G}$ , of which the element is calculated by (13).
- 6: Formulate the conditional Bernoulli probability distribution  $\text{Bern}(\mathbf{P}^{(i)})$  with probability  $P(\mathbf{W}_q^{(i)}(n, g) = 1) = p^{(i)}(n, g)$  subject to (11)-(12).
- 7: Sample new individuals  $\mathbf{W}_q^{(i)}$  from probability distribution  $\text{Bern}(\mathbf{P}^{(i)})$ , i.e.,  $\mathbf{W}_q^{(i)}(n, g) \sim \text{Bern}(p^{(i)}(n, g))$ .
- 8: Generate a new population  $\mathcal{W}^{(i)}$  with individuals  $\mathbf{W}_q^{(i)}, q = 1, \dots, Q$ .
- 9: Preserve the best individual  $\mathbf{W}_{\text{best}}^{(i-1)}$  from  $\mathcal{W}^{(i-1)}$  to  $\mathcal{W}^{(i)}$ , i.e.,  $\mathbf{W}_1^{(i)} = \mathbf{W}_{\text{best}}^{(i-1)}$ .
- 10: **end for**

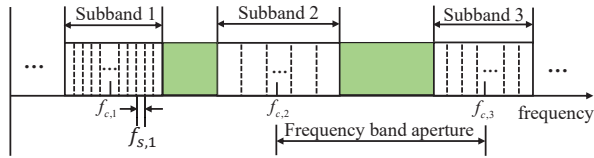


Fig. 6: Frequency distribution of the multiband system for pilot transmission.

the presence of frequency band apertures in multiband systems can be exploited to improve delay resolution of the system.

In this section, we extend our proposed multi-user pilot pattern optimization scheme to the multiband scenarios. We first formulate the multiband multi-user signal model. Then, we derive the performance metrics ISL and SRL based on the multiband multi-user signal model. Finally, the multiband multi-user pilot pattern optimization problem is formulated.

#### A. Multiband Signal Model

During the period of a single OFDM symbol, the multiband multi-user received signal model can be written as [22], [29]

$$y_{m,n}^{\text{MB}} = \sum_{g=1}^G \sum_{z=1}^Z \mathbf{h}_{g,z}^{\text{MB}}(m, n) \mathbf{w}_g^{\text{MB}}(m, n) \mathbf{x}_z^{\text{MB}}(m, n) + \mathbf{n}_{g,z}^{\text{MB}}(m, n), \quad (14)$$

where

$$\mathbf{h}_{g,z}^{\text{MB}}(m, n) = \sum_{k=1}^{K_{g,z}} \alpha_{g,z,k} e^{-j2\pi f_{m,n} \tau_{g,z,k}} e^{-j2\pi n f_{s,m} \delta_m} e^{j\varphi_m}$$

denotes the multiband CFR. The index  $(m, n)$  represents the  $n$ -th subcarrier of the  $m$ -th subband,  $m = 1, \dots, M, n \in \mathcal{N}_m \triangleq$

$\{-\frac{N_m-1}{2}, \dots, \frac{N_m-1}{2}\}$ ,  $f_{m,n} = f_{c,m} + n f_{s,m}$ . We assume that the subcarrier number of the  $m$ -th subband,  $N_m, \forall m$ , is an odd number without loss of generality, and denote  $N^{\text{MB}} = N_1 + \dots + N_M$  as the number of subcarriers over all subbands. The notations  $\mathbf{w}_g^{\text{MB}} \in \{0, 1\}^{N^{\text{MB}} \times 1}$  and  $\mathbf{x}_z^{\text{MB}} \in \mathbb{C}^{N^{\text{MB}} \times 1}$  denote the multiband pilot pattern vector of the  $g$ -th group and the  $z$ -th multiband SRS sequence, respectively.  $\mathbf{n}_{g,z}^{\text{MB}} \in \mathbb{C}^{N^{\text{MB}} \times 1}$  denotes the AWGN with each element having zero mean and variance  $\sigma_{n_s, g, z}^2$ . Due to the hardware imperfections, multiband systems are affected by two phase distortion factors, i.e., random phase offset  $\varphi_m$  and receiver timing offset  $\delta_m$ , which differ from band to band and need to be calibrated [30].

#### B. Problem Formulation

##### 1) Derivation of ISL in multiband multi-user scenarios:

In multiband scenarios, the AF of the  $(g, z)$ -th user can be derived as

$$\begin{aligned} \chi_{g,z}^{\text{MB}}(\Delta\tau) &= (\mathbf{w}_g^{\text{MB}} * \mathbf{x}_z^{\text{MB}} * \mathbf{a}^{\text{MB}}(\tau_1))^H (\mathbf{w}_g^{\text{MB}} * \mathbf{x}_z^{\text{MB}} * \mathbf{a}^{\text{MB}}(\tau_2)) \\ &= (\mathbf{w}_g^{\text{MB}})^T \mathbf{a}^{\text{MB}}(\Delta\tau), \end{aligned} \quad (15)$$

where  $\mathbf{a}^{\text{MB}}(\Delta\tau) \in \mathbb{C}^{N^{\text{MB}} \times 1}$  denotes the multiband frequency-domain steering vector consisting of the elements  $e^{-j2\pi f_{m,n} \Delta\tau - j2\pi n f_{s,m} \delta_m + \varphi_m}, \forall n, m$ . Then, substituting (15) into (4), the multiband ISL can be written as

$$\text{ISL}_g^{\text{MB}} = \frac{(\mathbf{w}_g^{\text{MB}})^T \mathbf{G}_g^{\text{MB}} \mathbf{w}_g^{\text{MB}}}{|\mathcal{R}_s| ((\mathbf{w}_g^{\text{MB}})^T \mathbf{1})^2}, \quad (16)$$

where

$$\mathbf{G}^{\text{MB}} = \begin{bmatrix} \mathbf{G}_{1,1} & \dots & \mathbf{G}_{1,M} \\ \vdots & \ddots & \vdots \\ \mathbf{G}_{M,1} & \dots & \mathbf{G}_{M,M} \end{bmatrix},$$

$$\mathbf{G}_{i,j}(n, l) = \frac{\sin(2\pi(f_{i,n} - f_{j,l})b) - \sin(2\pi(f_{i,n} - f_{j,l})a)}{\pi(f_{i,n} - f_{j,l})}.$$

Note that in multiband scenarios, the matrix  $\mathbf{G}^{\text{MB}}$  no longer preserves the Toeplitz structure in most cases.

2) Derivation of SRL in multiband multi-user scenarios: As compared to the SRL in single-band scenarios, the calculation of SRL in multi-user multiband scenarios requires the derivation of CRB based on the multiband signal model (14) in the presence of phase distortion factors.

To calculate SRL, we firstly need to derive the CRB for the delay separation  $\Delta\tau_{g,z}$ , which is given by

$$\text{CRB}_{\Delta\tau_{g,z}}^{\text{MB}} = \frac{\partial \Delta\tau_{g,z}}{\partial \boldsymbol{\eta}_{g,z}}^T \mathbf{J}_{\boldsymbol{\eta}_{g,z}}^{-1} \frac{\partial \Delta\tau_{g,z}}{\partial \boldsymbol{\eta}_{g,z}}, \quad (17)$$

where  $\mathbf{J}_{\boldsymbol{\eta}_{g,z}}$  is the FIM associated with the vector  $\boldsymbol{\eta}_{g,z} \triangleq [\boldsymbol{\theta}_{g,z}, \boldsymbol{\varphi}, \boldsymbol{\delta}]^T$ ,  $\boldsymbol{\varphi} = [\varphi_2, \dots, \varphi_M]^T$ ,  $\boldsymbol{\delta} = [\delta_1, \dots, \delta_M]^T$ . To avoid a singular FIM of  $\mathbf{J}_{\boldsymbol{\eta}_{g,z}}$ , we set  $f_{c,1} = 0, \varphi_1 = 0$ , and assume that  $\delta_m, \forall m$  follows a prior distribution  $p(\delta_m) \sim \mathcal{N}(0, \sigma_p^2)$  [22]. Then, from (17), we have

$$\text{CRB}_{\Delta\tau_{g,z}}^{\text{MB}} = \mathbf{J}_{\boldsymbol{\eta}_{g,z}}^{-1}(1, 1) + \mathbf{J}_{\boldsymbol{\eta}_{g,z}}^{-1}(2, 2) - \mathbf{J}_{\boldsymbol{\eta}_{g,z}}^{-1}(1, 2) - \mathbf{J}_{\boldsymbol{\eta}_{g,z}}^{-1}(2, 1),$$

where  $\mathbf{J}_{\eta_{g,z}} \triangleq \mathbf{J}_{g,z}^{(w)} + \mathbf{J}_{g,z}^{(p)}$ ,  $\mathbf{J}_{g,z}^{(w)}$  and  $\mathbf{J}_{g,z}^{(p)}$  are the FIMs from the observations and the a priori knowledge of  $\delta$ , respectively, which are defined as [31]

$$\mathbf{J}_{g,z}^{(w)} \triangleq \mathbb{E}_{\mathbf{y}^{\text{MB}}, \delta} \left[ -\frac{\partial^2 \ln f(\mathbf{y}^{\text{MB}} | \eta_{g,z})}{\partial \eta_{g,z} \partial \eta_{g,z}^T} \right],$$

$$\mathbf{J}_{g,z}^{(p)} \triangleq \mathbb{E}_{\delta} \left[ -\frac{\partial^2 \ln f(\delta)}{\partial \eta_{g,z} \partial \eta_{g,z}^T} \right].$$

The notation  $f(\delta) \propto \exp\{-\frac{\|\delta\|_2^2}{2\sigma_p^2}\}$  denotes the prior distribution of  $\delta$ . Furthermore,  $\mathbf{J}_{\eta_{g,z}}$  can be constructed as in (18). The entries in  $\mathbf{J}_{\eta_{g,z}}$  are derived in Appendix B.

3) *Problem formulation in multiband scenarios*: The optimization problem in multiband scenarios can be formulated as

$$\mathcal{P}^{\text{MB}} : \min_{\Xi} \max_g \{ \text{ISL}_g^{\text{MB}} \}$$

$$\text{s.t. } \text{SRL}_g^{\text{MB}} \leq \beta_g^{\text{MB}}, \forall g, \quad (19)$$

$$\sum_{g=1}^G \mathbf{w}_g^{\text{MB}} \leq \mathbf{1}, \quad (20)$$

where  $\Xi \triangleq \{\mathbf{w}_1^{\text{MB}}, \dots, \mathbf{w}_G^{\text{MB}}\}$  denotes the optimization variables set,  $\text{SRL}_g^{\text{MB}}$  denotes the multiband SRL of the  $g$ -th group, and  $\beta_g^{\text{MB}}$  denotes the upper limit on the multiband SRL of the  $g$ -th group. The multi-user multiband pilot optimization problem  $\mathcal{P}^{\text{MB}}$  can also be optimized in the offline manner using the EDA algorithm, which is similar to the offline optimization in single-band scenarios.

## V. SIMULATION RESULTS

In this section, we provide numerical results to validate the effectiveness of our proposed multi-user pilot pattern optimization scheme. In the default setup, the OFDM system is equipped with carrier frequency 3.5 GHz, the number of subcarriers  $N = 256$ , and the subcarrier spacing  $f_s = 120$  KHz. The SNR = 15 dB. We consider 4 users multiplexing in code-domain and frequency-domain for  $G = 2, Z = 2$ , as depicted in Fig. 5. Two users (User 1, User 2) transmit pilot symbols generated from a ZC sequence in set  $\Gamma$  to the BS with the optimized frequency-domain pilot pattern. The other two users (User 3, User 4) transmit pilot symbols with the same optimized pilot pattern as User 1 and User 2, but they employ another ZC sequence from the orthogonality set  $\Gamma$ . In EDA algorithm, we set  $\rho_{g,1} = \rho_{g,2} = 1$ ,  $\sigma_g = 0.1778, \forall g$ ,  $Q = 400, T = 200$ , and  $I = 60$ . The channel samples are generated by the QuaDRiGa toolbox [32] according to the 3D-Uma NLOS model defined by 3GPP R16 specifications [26].

For comparison, we consider the following two benchmark schemes, whose pilot patterns for 4 users have been shown in Fig. 5:

- **Baseline 1** (Uniform pilot pattern): Each user sequentially occupies a continuous segment of the frequency band with equivalent bandwidth. Take 4 users multiplexing for example: One user occupies the first half of the frequency band with evenly spaced pilot symbols, while the other

user occupies the second half of the frequency band with evenly spaced pilot symbols, too. The other two users adopt the same code-domain multiplexing method as the proposed scheme. This multi-user pilot pattern has been employed in current 5G NR systems.

- **Baseline 2** (Random pilot pattern): The users transmit pilot symbols with a random distribution in subcarriers. The code-domain multiplexing method is the same as the proposed scheme.

### A. Single-Band

We first illustrate the convergence behavior of the adopted EDA algorithm in multi-user pilot pattern optimization. As illustrated in Fig. 7, EDA converges within 50 iterations (up to a small convergence error). The optimized pilot pattern of the two users in frequency domain has been shown in Fig. 8. The pilot pattern for each user consists of two non-contiguous parts. Each part occupies the subcarriers with evenly spaced symbols. Besides, one part occupies the majority of the pilot symbols, while the other part only occupies the minority of the pilot symbols. This result can be justified that it takes into account the impact of both the employed metrics, SRL and ISL, in the optimization process. Specifically, the objective of minimizing ISL in  $\mathcal{P}$  requires the majority of pilot symbols for each user to be arranged as evenly spaced as possible. However, due to the SRL constraint in  $\mathcal{P}$ , the final pilot pattern cannot have all pilot symbols evenly spaced as Baseline 1 does. It has to separate out a small portion of pilot symbols to span a larger frequency range to satisfy the SRL requirement.

In Fig. 9, we present the AFs with regard to the optimized pilot pattern and baselines. As can be seen, the side-lobe level based on our proposed pilot pattern is much lower than that based on the random pilot pattern and it is nearly close to the side-lobe level based on the uniform pilot pattern. This phenomenon implies a superior multi-user interference mitigation capability of our proposed pilot pattern, as verified in Fig. 10, where the amplitude delay profiles are illustrated to show the impact of various pilot patterns on multi-user interference in code-domain multiplexing. As can be seen, the level of the multi-user interference of our proposed scheme is as low as the uniform pilot pattern scheme, and it is much lower than the random scheme.

Then, we compare the delay SRL values of our proposed pilot pattern scheme with the uniform pilot pattern scheme and the random pilot pattern scheme, which are 2.8882 ns, 5.7720 ns, and 2.9974 ns, respectively. It can be seen that our proposed pilot pattern scheme has much better SRL than the uniform pilot pattern scheme due to the effective delay SRL constraint (11) in  $\mathcal{P}$ .

Finally, we evaluate the channel extrapolation performance of the proposed pilot pattern and baselines using the particle swarm optimization-least square (PSO-LS) algorithm [22]. PSO-LS has a strong global search ability to find the optimal solution of a maximum likelihood (ML) estimation problem. In fact, PSO-LS is proposed for multiband delay estimation, which needs to solve a multi-dimensional multi-modal optimization problem that requires a robust global

$$\mathbf{J}_{\eta_{g,z}} = \begin{bmatrix} \Psi(\tau_{g,z}, \tau_{g,z}) & \Psi(\tau_{g,z}, \alpha_{g,z}) & \Psi(\tau_{g,z}, \varphi) & \Psi(\tau_{g,z}, \delta) \\ \Psi(\alpha_{g,z}, \tau_{g,z}) & \Psi(\alpha_{g,z}, \alpha_{g,z}) & \Psi(\alpha_{g,z}, \varphi) & \Psi(\alpha_{g,z}, \delta) \\ \Psi(\varphi, \tau_{g,z}) & \Psi(\varphi, \alpha_{g,z}) & \Psi(\varphi, \varphi) & \Psi(\varphi, \delta) \\ \Psi(\delta, \tau_{g,z}) & \Psi(\delta, \alpha_{g,z}) & \Psi(\delta, \varphi) & \Psi(\delta, \delta) \end{bmatrix}. \quad (18)$$

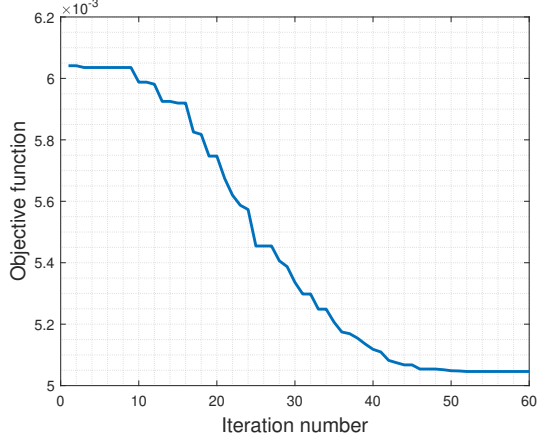


Fig. 7: Convergence behavior of the EDA algorithm in multi-user pilot pattern optimization.

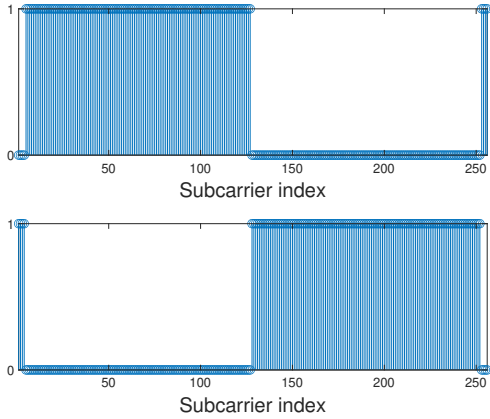


Fig. 8: An illustration of the optimized pilot pattern of two users for  $M = 1$ .

optimization ability. To have a proper initialization of the PSO-LS algorithm, e.g., determining the number of MPCs and the search range, the Turbo-CS algorithm has been employed as the initial phase estimator [22]. For fair comparison, we utilize the PSO-LS algorithm for channel extrapolation in both single-band and multiband scenarios.

Specifically, we first get the decoupled single-user observations  $\hat{\mathbf{y}}_{g,z}$  based on the multi-user interference cancellation procedure as depicted in Fig. 3. Then, we construct the ML estimation problem based on  $\hat{\mathbf{y}}_{g,z}$  as  $\min_{\alpha_{g,z,k}, \tau_{g,z,k}} \|\hat{\mathbf{y}}_{g,z} - \text{diag}(\mathbf{w}_g^{\text{opt}}) \mathbf{h}_{g,z}\|_2^2$ , where  $\mathbf{w}_g^{\text{opt}}$  denotes the optimized pilot pattern of the  $g$ -th group from the output of Algorithm 1. We solve it using PSO-LS to estimate the channel parameters  $\alpha_{g,z,k}, \tau_{g,z,k}$ . Finally, the full-band channel can be

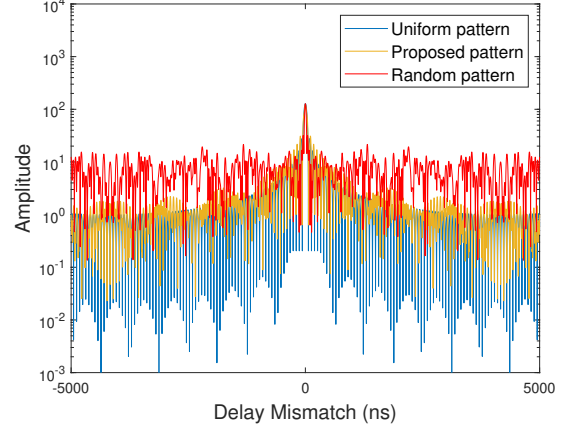


Fig. 9: An illustration of the AFs for  $M = 1$ .



Fig. 10: Amplitude delay profiles in delay domain for  $M = 1$ .

recovered based on the estimated channel parameters.

We choose NMSE as the performance metric to evaluate the channel extrapolation performance of various schemes, which is defined as

$$\text{NMSE} \triangleq \mathbb{E} \left\{ \frac{1}{GZ} \sum_{g=1}^G \sum_{z=1}^Z \frac{\|\hat{\mathbf{h}}_{g,z} - \mathbf{h}_{g,z}\|_2^2}{\|\mathbf{h}_{g,z}\|_2^2} \right\}, \quad (21)$$

where  $\hat{\mathbf{h}}_{g,z}$  is the estimate of  $\mathbf{h}_{g,z}$ , the expectations in (21) are computed by averaging over 500 Monte Carlo trials. As shown in Fig. 11, the scheme based on the proposed pilot pattern has the lowest NMSE of channel extrapolation as compared to baselines. Besides, the performance gap between our proposed scheme and the uniform pilot pattern scheme is larger in lower SNR region.

In summary, though uniform pilot pattern scheme has strong code-domain multiplexing capability with effective multi-user

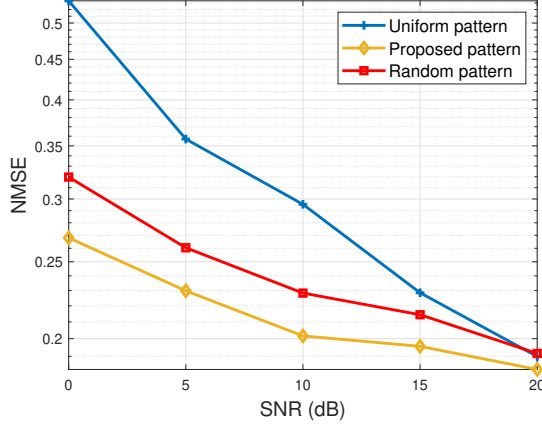


Fig. 11: NMSE of the full-band channel versus SNR for  $M = 1$ .

interference cancellation, its drawback lies in its insufficient delay resolution and thus results in poor channel extrapolation performance. On the other hand, though random pilot pattern leads to sufficient delay resolution of the system, but it suffers from severe multi-user interference in code-domain multiplexing, and due to the high level side-lobe of AF causing significant delay ambiguity, the accuracy of delay estimation is limited. In contrast to these two baselines, our proposed pilot pattern scheme has both the advantages of robust resistance to multi-user interference and the high resolution delay estimation. Consequently, the overall channel extrapolation performance of the proposed scheme is better than that of the baseline schemes.

### B. Multiband

In multiband scenarios of the default setup, the OFDM system is equipped with carrier frequency  $f_{c,1} = 3.5$  GHz,  $f_{c,2} = 3.9$  GHz, the number of subcarriers  $N_1 = N_2 = 128$ , and the subcarrier spacing  $f_{s,1} = f_{s,2} = 120$  KHz at  $M = 2$  subbands. We consider 2 users ( $G = 2, Z = 2$ ) and 3 users ( $G = 3, Z = 2$ ) multiplexing in frequency-domain, respectively, and for the case of  $G = 3$ , we set  $N_1 = N_2 = 192$ .

The optimized pilot pattern has been shown in Fig. 12a, where the pilot symbols of each user are arranged in both subbands. Moreover, in each subband, the pilot symbols are evenly spaced. This pilot pattern is rational since it ensures the majority of pilot symbols evenly spaced to reduce the multi-user interference and simultaneously spans two subbands to reserve the frequency band aperture structure (which is the source of the multiband gains) to improve delay resolution of the system. In Fig. 12b, we can see that all three users have arranged the pilot symbols into two subbands, and in each subband, the pilot symbols are evenly spaced as the case  $G = 2$  does.

We plot the curve of AF in Fig. 13. It can be seen that the the proposed pilot pattern still achieves a lower side-lobe level than the random pilot pattern as that in single-

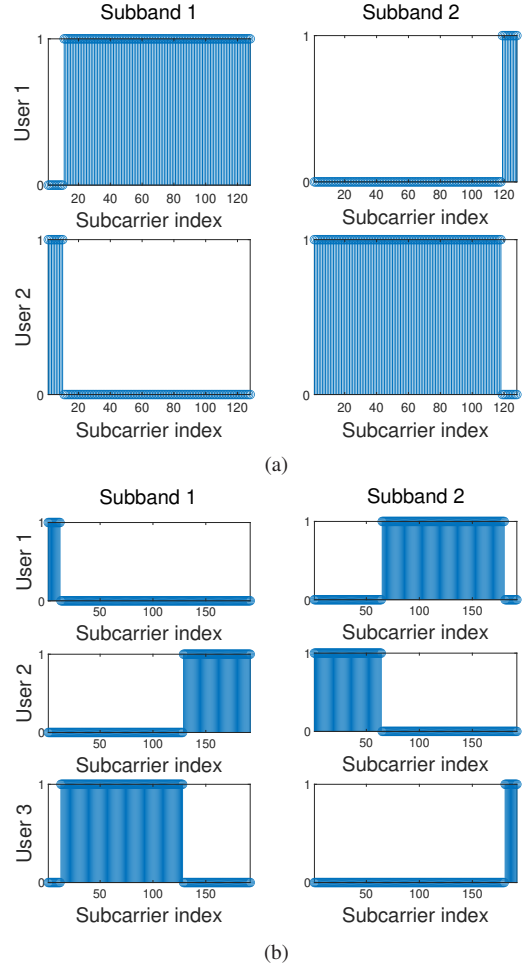


Fig. 12: An illustration of the optimized pilot pattern for  $M = 2$ : (a)  $G = 2$ ; (b)  $G = 3$ .

band scenarios. Moreover, in multiband scenarios, the side-lobe fluctuates more frequently compared with that in single-band scenarios. It can be justified that in the multiband AF expression (15), the delay mismatch  $\Delta\tau$  is multiplied by a high carrier frequency  $f_{c,m}$ . Consequently, a slight variation of  $\Delta\tau$  may lead to a significant phase shift of  $a^{\text{MB}}(\Delta\tau)$  and finally it is reflected in the violent oscillation of the AF.

Then, we calculate the delay SRL values of our proposed pilot pattern scheme, the uniform pilot pattern scheme, and the random pilot pattern scheme for the case of  $G = 2$ , which are 0.5707 ns, 5.7977 ns, and 0.5844 ns, respectively. It can be seen that the SRL of our proposed pilot pattern scheme and the random pilot pattern scheme in multiband scenarios is much better than that in single-band scenarios due to the multiband gains brought by the inherent frequency band apertures in multiband systems. The uniform pilot pattern scheme, however, does not reserve the frequency band aperture structure since the pilots of each user only occupy a single contiguous subband. Consequently, the SRL of the uniform pilot pattern scheme has not been significantly improved. In Fig. 14, we investigate the extrapolation performance of the proposed pilot pattern scheme. As can be seen, in multiband

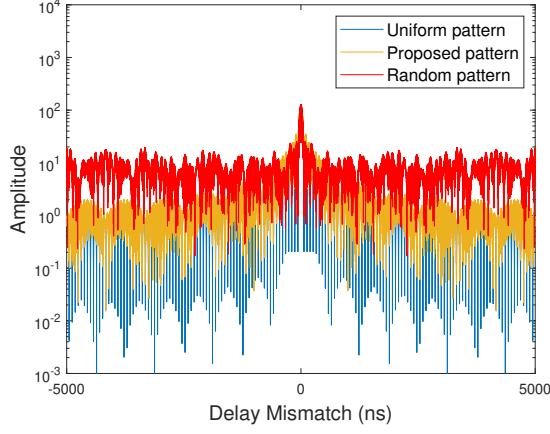


Fig. 13: An illustration of the AFs for  $M = 2$ .

scenarios, both the schemes based on the random pilot pattern and the proposed pilot pattern have a lower NMSE than the uniform pilot pattern scheme. As stated of the delay SRL comparison earlier, the system based on these two pilot patterns has sufficient delay resolution owing to the exploitation of multiband gains. The scheme based on the uniform pilot pattern, however, does not reserve the frequency band aperture structure for any user and thus cannot exploit the multiband gains to improve delay resolution of the system.

Furthermore, compare the NMSE performance of our proposed scheme in Fig. 14a to that in Fig. 11, it can be seen that the channel extrapolation performance of the proposed pilot pattern scheme is better in multiband scenarios than in single-band scenarios, which validates the effective leverage of the multiband gains to improve the channel extrapolation performance by the proposed pilot pattern scheme.

## VI. CONCLUSION

In this paper, we have designed a multi-user pilot pattern for channel extrapolation in OFDM systems. We have formulated an offline multi-user pilot pattern optimization problem with the objective of minimizing the maximum ISL among users. By doing this, the multi-user interference can be well mitigated in code-domain and the side-lobe of the AF is significantly suppressed. Besides, we have considered a constraint of the SRL of the system to ensure that it has sufficient delay resolution for channel extrapolation. Furthermore, we have extended our pilot pattern optimization scheme to a multiband scenario for the sake of exploiting the multiband gain to improve delay resolution of the system. Finally, simulation results show that our proposed pilot pattern outperforms the baselines for channel extrapolation performance in both single-band and multiband scenarios. The optimized pilot patterns provide useful guidance for the design of multi-user pilot pattern in 5G NR systems.

### APPENDIX

#### A. Derivation of $\mathbf{J}_{\theta_{g,z}}$

The FIM  $\mathbf{J}_{\theta_{g,z}}$  can be structured as

$$\mathbf{J}_{\theta_{g,z}} = \begin{bmatrix} \Phi(\boldsymbol{\tau}_{g,z}, \boldsymbol{\tau}_{g,z}) & \Phi(\boldsymbol{\tau}_{g,z}, \boldsymbol{\alpha}_{g,z}) \\ \Phi(\boldsymbol{\alpha}_{g,z}, \boldsymbol{\tau}_{g,z}) & \Phi(\boldsymbol{\alpha}_{g,z}, \boldsymbol{\alpha}_{g,z}) \end{bmatrix}. \quad (22)$$

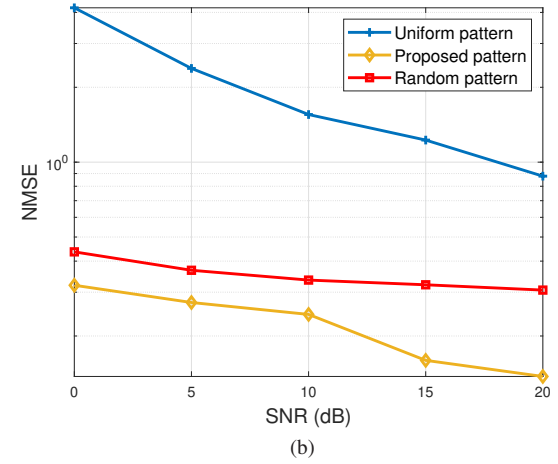
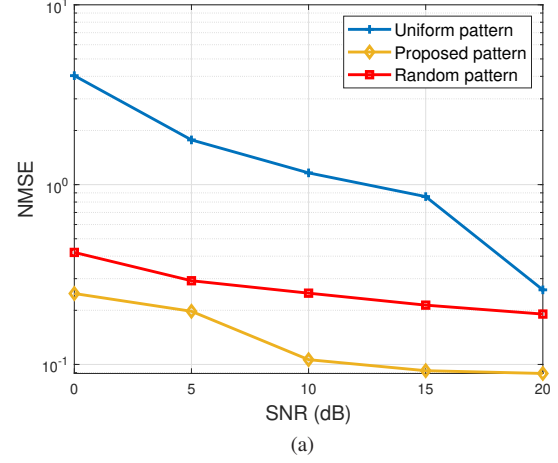


Fig. 14: NMSE of the full-band channel versus SNR for  $M = 2$ : (a)  $G = 2$ ; (b)  $G = 3$ .

For easy of illustration, we omit the subscript  $(g, z)$  in the expression of the entries in  $\mathbf{J}_{\theta_{g,z}}$ . The expression is given by

$$\begin{aligned} \Phi(\tau_r, \tau_s) &= \frac{8\pi^2}{\sigma_e^2} \sum_n (nf_s)^2 \text{Re} \left\{ (\alpha'_r)^* \alpha'_s e^{j2\pi n f_s (\tau_r - \tau_s)} \mathbf{w}(n) \right\}, \\ \Phi(\tau_r, \alpha_s^R) &= \Phi(\alpha_s^R, \tau_r) \\ &= \frac{4\pi}{\sigma_e^2} \sum_n \text{Re} \left\{ jnf_s (\alpha'_r)^* e^{j2\pi n f_s (\tau_r - \tau_s)} \mathbf{w}(n) \right\}, \\ \Phi(\tau_r, \alpha_s^I) &= \Phi(\alpha_s^I, \tau_r), \\ &= -\frac{4\pi}{\sigma_e^2} \sum_n \text{Re} \left\{ nf_s (\alpha'_r)^* e^{j2\pi n f_s (\tau_r - \tau_s)} \mathbf{w}(n) \right\} \\ \Phi(\alpha_r^R, \alpha_s^R) &= \Phi(\alpha_r^I, \alpha_s^I) = \frac{2}{\sigma_e^2} \sum_n \cos(2\pi n f_s (\tau_r - \tau_s)) \mathbf{w}(n), \\ \Phi(\alpha_r^R, \alpha_s^I) &= -\Phi(\alpha_r^I, \alpha_s^R) = \frac{2}{\sigma_e^2} \sum_n \sin(2\pi n f_s (\tau_s - \tau_r)) \mathbf{w}(n), \end{aligned}$$

where  $r = 1, 2, s = 1, 2$ .

### B. Entries in $\mathbf{J}_{\eta_{g,z}}$

For easy of illustration, we also omit the subscript  $(g, z)$  in the expression of the entries, which are written as

$$\begin{aligned}
\Psi(\tau_r, \tau_s) &= \frac{8\pi^2}{\sigma_{ns}^2} \sum_{m,n} f_{m,n}^2 \operatorname{Re} \left\{ (\alpha'_r)^* \alpha'_s e^{j2\pi f_{m,n}(\tau_r - \tau_s)} \mathbf{w}^{\text{MB}}(m, n) \right\}, \\
\Psi(\tau_r, \alpha_s^R) &= \frac{4\pi}{\sigma_{ns}^2} \sum_{m,n} \operatorname{Re} \left\{ j f_{m,n} (\alpha'_r)^* e^{j2\pi f_{m,n}(\tau_r - \tau_s)} \mathbf{w}^{\text{MB}}(m, n) \right\}, \\
\Psi(\tau_r, \alpha_s^I) &= -\frac{4\pi}{\sigma_{ns}^2} \sum_{m,n} \operatorname{Re} \left\{ f_{m,n} (\alpha'_r)^* e^{j2\pi f_{m,n}(\tau_r - \tau_s)} \mathbf{w}^{\text{MB}}(m, n) \right\}, \\
\Psi(\tau_r, \varphi'_i) &= -\frac{4\pi}{\sigma_{ns}^2} \sum_{n,m=i} \operatorname{Re} \left\{ f_{i,n} (\alpha'_r)^* \sum_{k=1}^K \alpha'_k e^{j2\pi f_{i,n}(\tau_r - \tau_k)} \mathbf{w}^{\text{MB}}(m, n) \right\}, \\
\Psi(\tau_r, \delta_i) &= \frac{8\pi^2}{\sigma_{ns}^2} \sum_{n,m=i} n f_{i,n} f_{s,i} \operatorname{Re} \left\{ (\alpha'_r)^* \sum_{k=1}^K \alpha'_k e^{j2\pi f_{i,n}(\tau_r - \tau_k)} \mathbf{w}^{\text{MB}}(m, n) \right\}, \\
\Psi(\alpha_r^R, \alpha_s^R) &= \Psi(\alpha_r^I, \alpha_s^I) \\
&= \frac{2}{\sigma_{ns}^2} \sum_{m,n} \cos(2\pi f_{m,n}(\tau_r - \tau_s)) \mathbf{w}^{\text{MB}}(m, n), \\
\Psi(\alpha_r^R, \alpha_s^I) &= -\Psi(\alpha_r^I, \alpha_s^R) \\
&= \frac{2}{\sigma_{ns}^2} \sum_{m,n} \sin(2\pi f_{m,n}(\tau_s - \tau_r)) \mathbf{w}^{\text{MB}}(m, n), \\
\Psi(\alpha_r^R, \varphi'_i) &= \frac{2}{\sigma_{ns}^2} \sum_{n,m=i} \operatorname{Re} \left\{ j \sum_{k=1}^K \alpha'_k e^{j2\pi f_{i,n}(\tau_r - \tau_k)} \mathbf{w}^{\text{MB}}(m, n) \right\}, \\
\Psi(\alpha_r^R, \delta_i) &= -\frac{4\pi}{\sigma_{ns}^2} \sum_{n,m=i} \operatorname{Re} \left\{ j n f_{s,i} \sum_{k=1}^K \alpha'_k e^{j2\pi f_{i,n}(\tau_r - \tau_k)} \mathbf{w}^{\text{MB}}(m, n) \right\}, \\
\Psi(\alpha_r^I, \varphi'_i) &= \frac{2}{\sigma_{ns}^2} \sum_{n,m=i} \operatorname{Re} \left\{ \sum_{k=1}^K \alpha'_k e^{j2\pi f_{i,n}(\tau_r - \tau_k)} \mathbf{w}^{\text{MB}}(m, n) \right\}, \\
\Psi(\alpha_r^I, \delta_i) &= -\frac{4\pi}{\sigma_{ns}^2} \sum_{n,m=i} \operatorname{Re} \left\{ n f_{s,i} \sum_{k=1}^K \alpha'_k e^{j2\pi f_{i,n}(\tau_r - \tau_k)} \mathbf{w}^{\text{MB}}(m, n) \right\}, \\
\Psi(\varphi'_r, \varphi'_s) &= \begin{cases} \frac{8\pi^2}{\sigma_{ns}^2} \sum_{n,m=r} n^2 f_{s,r}^2 \left| \sum_{k=1}^K \alpha'_k e^{-j2\pi f_{r,n} \tau_k} \right|^2 \\ \quad \times \mathbf{w}^{\text{MB}}(m, n), r = s, \\ 0, \text{ otherwise,} \end{cases} \\
\Psi(\varphi'_r, \delta_s) &= \begin{cases} -\frac{4\pi}{\sigma_{ns}^2} \sum_{n,m=r} n f_{s,r} \left| \sum_{k=1}^K \alpha'_k e^{-j2\pi f_{r,n} \tau_k} \right|^2 \\ \quad \times \mathbf{w}^{\text{MB}}(m, n), r = s, \\ 0, \text{ otherwise,} \end{cases}
\end{aligned}$$

$$\Psi(\delta_r, \delta_s) = \begin{cases} \frac{8\pi^2}{\sigma_{ns}^2} \sum_{n,m=r} n^2 f_{s,r}^2 \left| \sum_{k=1}^K \alpha'_k e^{-j2\pi f_{r,n} \tau_k} \right|^2 \\ \quad \times \mathbf{w}^{\text{MB}}(m, n) + \frac{1}{\sigma_p^2}, r = s, \\ 0, \text{ otherwise.} \end{cases} \quad (23)$$

### REFERENCES

- [1] L. Cimini, "Analysis and simulation of a digital mobile channel using orthogonal frequency division multiplexing," *IEEE Trans. Commun.*, vol. 33, no. 7, pp. 665–675, 1985.
- [2] *3GPP, TS 38.211 V16.7.0 Release 16, Technical Specification Group Radio Access Network; NR; Physical channels and modulation*, Sep. 2021.
- [3] F. Rottenberg, T. Choi, P. Luo, C. J. Zhang, and A. F. Molisch, "Performance analysis of channel extrapolation in FDD massive MIMO systems," *IEEE Trans. Wireless Commun.*, vol. 19, no. 4, pp. 2728–2741, Apr. 2020.
- [4] M.-O. Pun, A. F. Molisch, P. Orlik, and A. Okazaki, "Super-resolution blind channel modeling," in *Proc. IEEE Int. Conf. Commun. (ICC)*, Jun. 2011, pp. 1–5.
- [5] N. Jalden, H. Asplund, and J. Medbo, "Channel extrapolation based on wideband MIMO measurements," in *Proc. 6th Eur. Conf. Antennas Propag. (EUCAP)*, Mar. 2012, pp. 442–446.
- [6] X. Xu, S. Zhang, F. Gao, and J. Wang, "Sparse Bayesian learning based channel extrapolation for RIS assisted MIMO-OFDM," *IEEE Trans. Commun.*, vol. 70, no. 8, pp. 5498–5513, Aug. 2022.
- [7] Y. Han, S. Jin, X. Li, C.-K. Wen, and T. Q. S. Quek, "Multi-domain channel extrapolation for FDD massive MIMO systems," *IEEE Trans. Commun.*, vol. 69, no. 12, pp. 8534–8550, Dec. 2021.
- [8] Y. Wan and A. Liu, "A two-stage 2D channel extrapolation scheme for TDD 5G NR systems," *IEEE Trans. Wireless Commun. (Early Access)*, pp. 1–1, 2024.
- [9] M. Simko, P. S. R. Diniz, Q. Wang, and M. Rupp, "Adaptive pilot-symbol patterns for MIMO OFDM systems," *IEEE Trans. Wireless Commun.*, vol. 12, no. 9, pp. 4705–4715, Sep. 2013.
- [10] W. Zhang, X.-G. Xia, and P. C. Ching, "Optimal training and pilot pattern design for OFDM systems in rayleigh fading," *IEEE Trans. Broadcast.*, vol. 52, no. 4, pp. 505–514, 2006.
- [11] I. Barhumi, G. Leus, and M. Moonen, "Optimal training design for MIMO OFDM systems in mobile wireless channels," *IEEE Trans. Signal Process.*, vol. 51, no. 6, pp. 1615–1624, Jun. 2003.
- [12] M. A. Youssefi and J. El Abbadi, "Pilot-symbol patterns for MIMO OFDM systems under time varying channels," in *2015 International Conference on Electrical and Information Technologies (ICEIT)*, Mar. 2015, pp. 322–328.
- [13] J.-C. Chen, C.-K. Wen, and P. Ting, "An efficient pilot design scheme for sparse channel estimation in OFDM systems," *IEEE Commun. Lett.*, vol. 17, no. 7, pp. 1352–1355, Jul. 2013.
- [14] C.-H. Kim and Y.-H. Lee, "Adaptive pilot signaling in the uplink of OFDM-based wireless systems," in *2007 16th IST Mobile and Wireless Communications Summit*, Jul. 2007, pp. 1–5.
- [15] Z. Sheng, H. D. Tuan, H. H. Nguyen, and Y. Fang, "Pilot optimization for estimation of high-mobility OFDM channels," *IEEE Trans. Veh. Technol.*, vol. 66, no. 10, pp. 8795–8806, Oct. 2017.
- [16] H. Wang, Q. Guo, G. Zhang, G. Li, and W. Xiang, "Pilot pattern optimization for sparse channel estimation in OFDM systems," *IEEE Commun. Lett.*, vol. 19, no. 7, pp. 1233–1236, Jul. 2015.
- [17] C. Qi, G. Yue, L. Wu, and A. Nallanathan, "Pilot design for sparse channel estimation in OFDM-based cognitive radio systems," *IEEE Trans. Veh. Technol.*, vol. 63, no. 2, pp. 982–987, Feb. 2014.
- [18] C. Qi and L. Wu, "Optimized pilot placement for sparse channel estimation in OFDM systems," *IEEE Signal Processing Letters*, vol. 18, no. 12, pp. 749–752, Dec. 2011.
- [19] X. He and R. Song, "Pilot pattern optimization for compressed sensing based sparse channel estimation in OFDM systems," in *2010 International Conference on Wireless Communications Signal Processing (WCSP)*, Oct. 2010, pp. 1–5.
- [20] H. Al-Salihi, T. Van Chien, T. A. Le, and M. R. Nakhai, "A successive optimization approach to pilot design for multi-cell massive MIMO systems," *IEEE Commun. Lett.*, vol. 22, no. 5, pp. 1086–1089, May. 2018.
- [21] T. Kazaz *et al.*, "Delay estimation for ranging and localization using multiband channel state information," *IEEE Trans. Wireless Commun.*, vol. 21, no. 4, pp. 2591–2607, Apr. 2022.

- [22] Y. Wan, A. Liu, Q. Hu, M. Zhang, and Y. Cai, "Multiband delay estimation for localization using a two-stage global estimation scheme," *IEEE Trans. Wireless Commun.*, vol. 22, no. 12, pp. 9263–9277, Dec. 2023.
- [23] M. F. Keskin, V. Koivunen, and H. Wymeersch, "Limited feedforward waveform design for OFDM dual-functional radar-communications," *IEEE Trans. Signal Process.*, vol. 69, pp. 2955–2970, Apr. 2021.
- [24] S. Smith, "Statistical resolution limits and the complexified Cramer-Rao bound," *IEEE Trans. Signal Process.*, vol. 53, no. 5, pp. 1597–1609, May. 2005.
- [25] J. Zhang, H. Wang, and X. Zhu, "Adaptive waveform design for separated transmit/receive ULA-MIMO radar," *IEEE Trans. Signal Process.*, vol. 58, no. 9, pp. 4936–4942, Sep. 2010.
- [26] 3GPP, "Study on channel model for frequencies from 0.5 to 100 GHz (3GPP TR 38.901 version 16.1.0 release 16)," Dec. 2019.
- [27] C. Gao, K. C. Teh, and A. Liu, "Piecewise nonlinear frequency modulation waveform for MIMO radar," *IEEE Journal of Selected Topics in Signal Processing*, vol. 11, no. 2, pp. 379–390, Mar. 2017.
- [28] S. K. Sengijpta, "Fundamentals of statistical signal processing: Estimation theory," 1995.
- [29] M. B. Khalilsarai, B. Gross, S. Stefanatos, G. Wunder, and G. Caire, "WiFi-based channel impulse response estimation and localization via multi-band splicing," in *Proc. IEEE Global Commun. Conf. (GLOBECOM)*, Dec. 2020, pp. 1–6.
- [30] Y. Xie, Z. Li, and M. Li, "Precise power delay profiling with commodity Wi-Fi," *IEEE Trans. Mobile Comput.*, vol. 18, no. 6, pp. 1342–1355, Jun. 2019.
- [31] P. Tichavsky, C. Muravchik, and A. Nehorai, "Posterior Cramer-Rao bounds for discrete-time nonlinear filtering," *IEEE Trans. Signal Process.*, vol. 46, no. 5, pp. 1386–1396, May. 1998.
- [32] S. Jaeckel, L. Raschkowski, K. Borner, and L. Thiele, "Quadriga: A 3-D multi-cell channel model with time evolution for enabling virtual field trials," *IEEE Trans. Antennas Propag.*, vol. 62, no. 6, pp. 3242–3256, Jun. 2014.

This figure "systemModel.jpg" is available in "jpg" format from:

<http://arxiv.org/ps/2407.10532v1>